

Supporting Information for

# The Diradicaloid Electronic Structure of Dialumenes: a Benchmark Study at the Full-CI Limit

Keelan M. Byrne<sup>1</sup>, Ragnar Bjornsson<sup>3,\*</sup>, Tobias Krämer<sup>1,2,\*</sup>

<sup>1</sup> Department of Chemistry, Maynooth University, Maynooth, Co. Kildare, Ireland

<sup>2</sup> Hamilton Institute, Maynooth University, Maynooth, Co, Kildare, Ireland

<sup>3</sup> Univ. Grenoble Alpes, CNRS, CEA, IRIG, Laboratoire de Chimie et Biologie des Métaux, 17 Rue des Martyrs,  
F-38054 Grenoble, Cedex, France

Correspondence to: [ragnar.bjornsson@cea.fr](mailto:ragnar.bjornsson@cea.fr) and [tobias.kraemer@mu.ie](mailto:tobias.kraemer@mu.ie)

## Additional data on Al<sub>2</sub>H<sub>2</sub>

### The impact of the reference WF in CC calculations

Table S1 shows the largest singles and doubles amplitudes for RHF-CCSD and UHF-CCSD wavefunctions of Al<sub>2</sub>H<sub>2</sub>.

**Table S1** The 8 largest CCSD amplitudes for each of the reference wavefunctions in Table S1. The orbital indices for each excitation are included in rounded brackets (HOMO = Orbital 14). Basis set is cc-pVTZ.

Wavefunction	Excitation	Amplitude
<i>RHF (Unstable)</i>	Double (14 → 16, 14 → 16)	0.203006
	Double (14 → 15, 14 → 15)	0.071403
	Double (14 → 27, 14 → 16)	0.054717
	Double (14 → 16, 14 → 27)	0.054717
	Single (13 → 16)	0.046911
	Double (13 → 19, 13 → 19)	0.043236
	Double (13 → 15, 13 → 15)	0.040864
	Double (14 → 20, 14 → 16)	0.038510
<i>UHF (Stable)</i>	Single (14b → 16b)	0.285523
	Single (14a → 16a)	0.285523
	Double (14a → 16a, 14b → 16b)	0.207040
	Double (14a → 15a, 14b → 15b)	0.055027

	Double (14a → 16a, 14b → 30b)	0.051242
	Double (14a → 30a, 14b → 16b)	0.051242
	Single (14b → 30b)	0.049036
	Single (14a → 30a)	0.049036
<i>RKS B3LYP (Stable)</i>	Double (14 → 16, 14 → 16)	0.201767
	Double (14 → 15, 14 → 15)	0.069560
	Double (14 → 27, 14 → 16)	0.055328
	Double (14 → 16, 14 → 27)	0.055328
	Double (13 → 19, 13 → 19)	0.041760
	Double (13 → 15, 13 → 15)	0.040361
	Double (14 → 16, 14 → 20)	0.037432
	Double (14 → 20, 14 → 16)	0.037432

### **Basis set convergence of the vertical bond dissociation energy**

The basis set dependence of the vertical bond dissociation (VBDE) was explored by CCSD(T) calculations with cc-pVnZ basis sets where  $n = T, Q, 5$  as shown in Figure S1. A CBS(4,5) extrapolation is also shown.

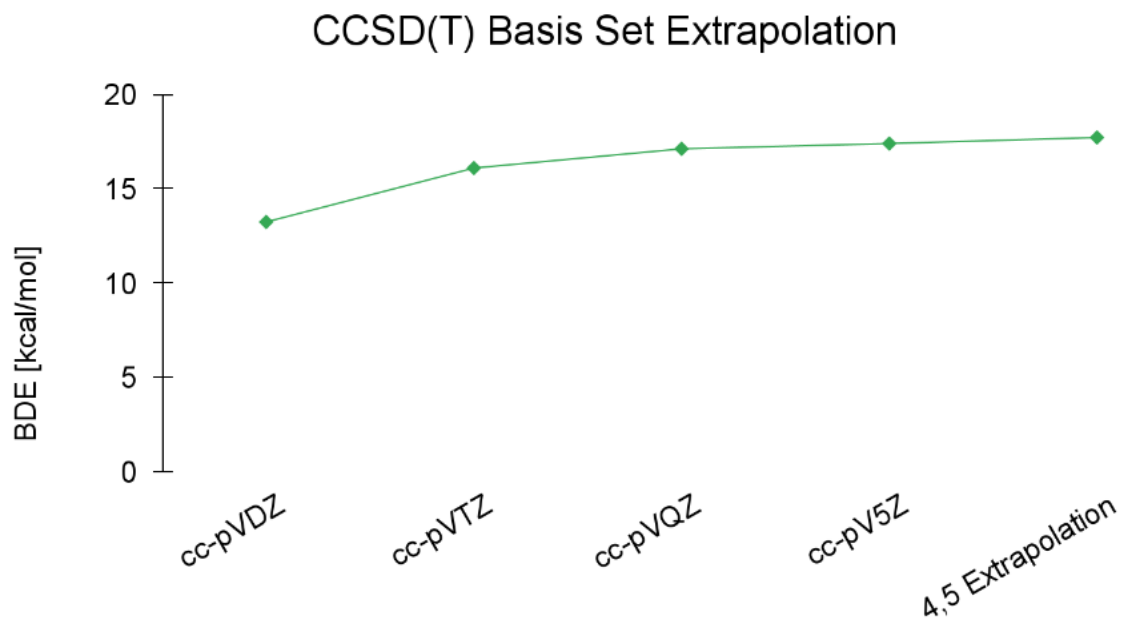


**Fig. S1** Convergence of the  $\text{Al}_2\text{H}_2$  vertical bond dissociation energy at the RHF-CCSD(T) level as a function of basis set size. Also shown is a basis set extrapolation of the bond dissociation energy using the cc-pVQZ and cc-pV5Z energies. A TZ→CBS correction of 1.62 kcal/mol (i.e. BDE[4,5 Extrapolation] - BDE[cc-pVTZ]) can be derived from these values.

### Convergence of SHCI wavefunction with and without perturbation correction

The SHCI selected CI WF calculations of the VBDE could be carried out with or without a perturbation correction. Figure S2 compares the convergence of using the correction or not. While both procedures appear to converge to the same limit, the PT correction makes a large difference in converging more quickly.

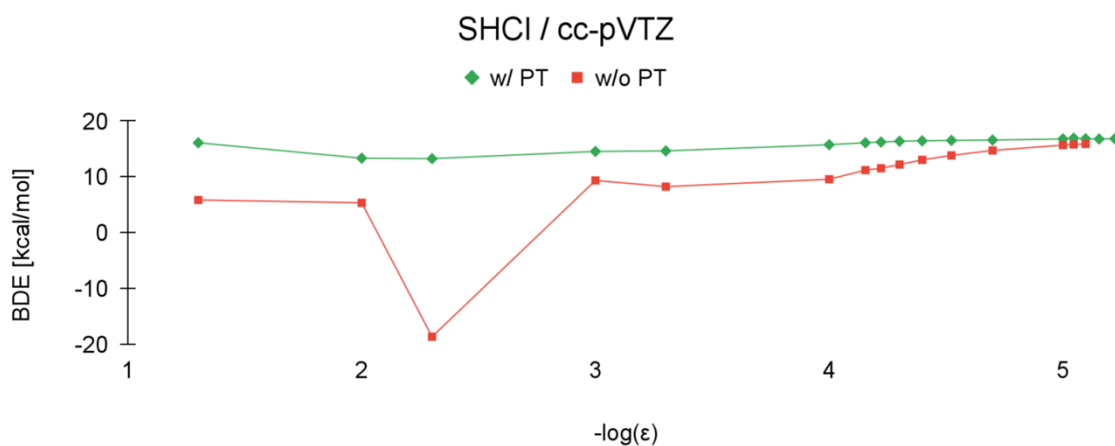


**Fig. S2** Bond dissociation energy of  $\text{Al}_2\text{H}_2$  using the SHCI method, with and without a perturbation theory correction, as a function of the  $\epsilon$  SHCI selection parameter. An active space of (8,86) was used (corresponds to Full-CI with a frozen-core approximation). CCSD natural orbitals were used as the input orbitals and the basis set is cc-pVTZ.

## Vertical bond dissociation energy with additional methods

The VBDE of  $\text{Al}_2\text{H}_2$  was also calculated with a few additional methods as shown in Table S2, namely alternative perturbation theory methods and CC with a Kohn-Sham(B3LYP) reference determinant. Neither SCS-MP2 or OO-RI-MP2 are found to improve upon regular MP2 and neither does MP3 or SCS-MP3. The use of a Kohn-Sham determinant does not result in improved CCSD or CCSD(T) energies (compared to RHF-CCSD and RHF-CCSD(T)).

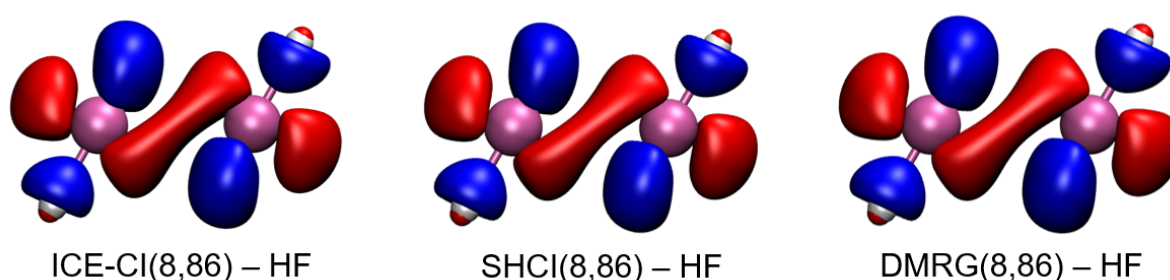
**Table S2** The vertical bond dissociation energy of  $\text{Al}_2\text{H}_2$  with additional wavefunction methods using the cc-pVTZ basis set.

	VBDE [kcal mol <sup>-1</sup> ]
RKS(B3LYP)-CCSD <sup>a</sup>	12.89
RKS(B3LYP)-CCSD(T) <sup>a</sup>	15.95
SCS-MP2	13.34
OO-RI-MP2	18.69
MP3	15.69
SCS-MP3	13.33

<sup>a</sup> A restricted Kohn-Sham (B3LYP) reference determinant was used.

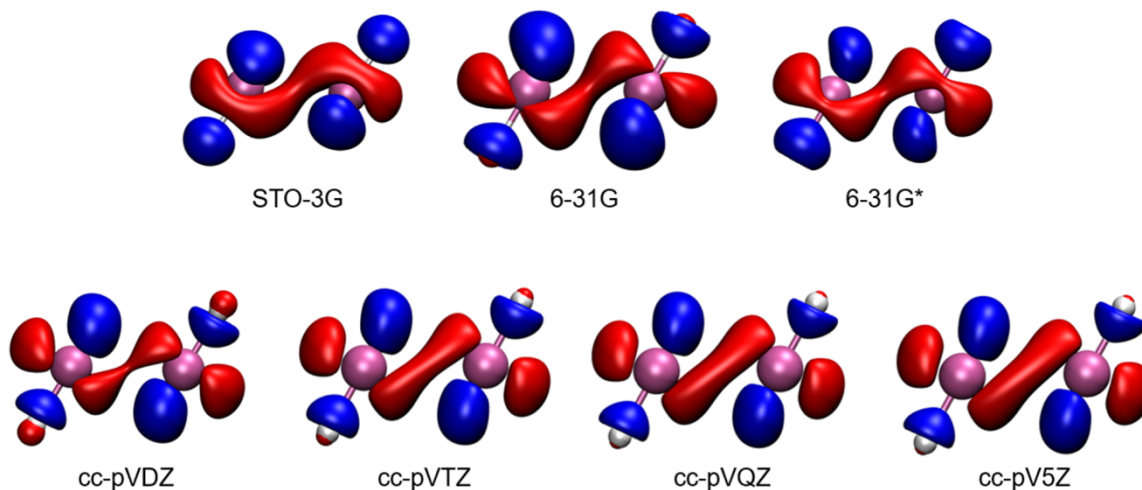
## Additional difference density plots

Figure S3 shows a comparison of the difference density plots (relative to RHF) of the near-Full-CI methods DMRG, ICE-CI and SHCI, revealing that all 3 methods are capable of giving near-identical estimates of the Full-CI density. All methods used the same active space of (8,86) and CCSD natural orbitals.



**Fig. S3** Comparison of difference density plots of DMRG ( $M = 920$ ), SHCI( $\epsilon = 6 \times 10^{-6}$ ) and ICE-CI( $T_{\text{Gen}} = 4 \times 10^{-5}$ ) densities, relative to the RHF density. Red indicates an accumulation of density in going from RHF to ICE-CI/SHCI/DMRG while blue indicates a depletion of density (isovalue =  $\pm 0.001$ ).

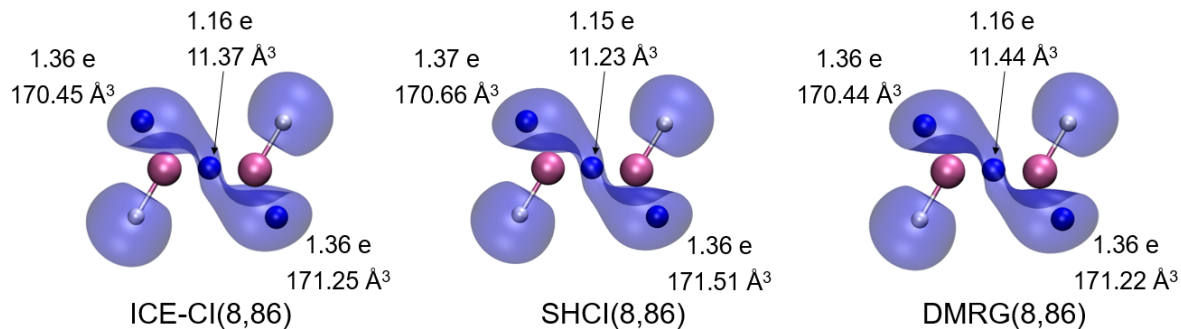
Figure S4 compares the basis set dependency of the difference density plots at the unrelaxed CCSD density level. The density is overall found to be well converged at the cc-pVTZ level.



**Fig. S4** Convergence of the CCSD-RHF difference density for basis sets of increasing size/complexity. The difference density between the unrelaxed RHF-CCSD and RHF density was used to demonstrate the convergence of the difference density with respect to basis set size. **Red** indicates an accumulation of density w.r.t. RHF, and **blue** indicates a depletion of density (isovalue =  $\pm 0.001$ ).

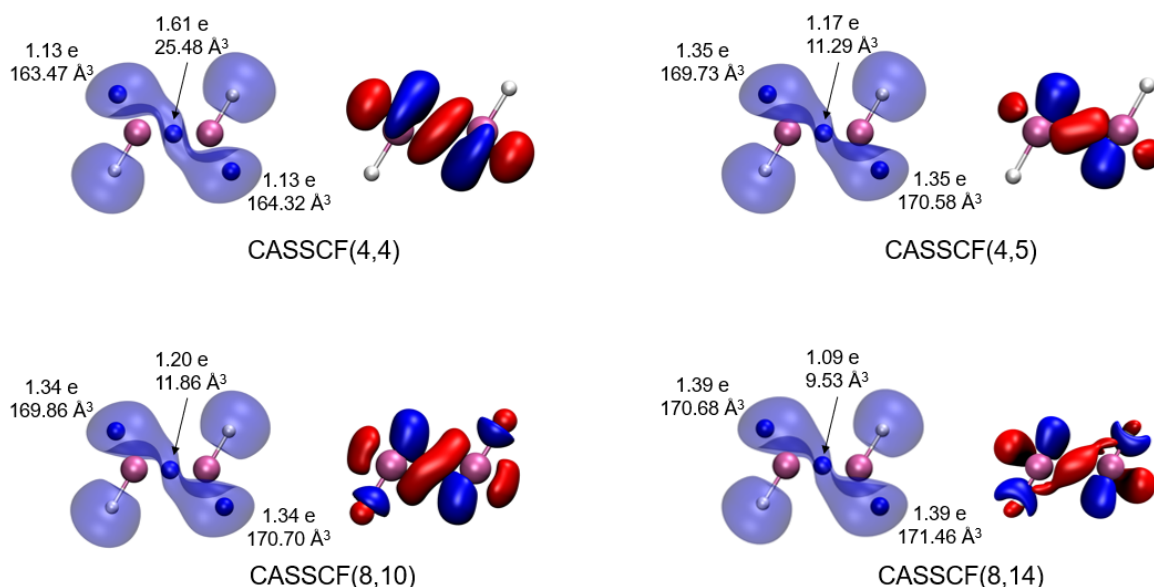
### Additional ELF plots

Figure S5 shows a comparison of the ELF plots with the near-Full-CI methods DMRG, ICE-CI and SHCI, revealing that all 3 methods are capable of giving near-identical estimates of the Full-CI electron localization function plot and integrated basin populations.



**Fig. S5** Plots of the electron localisation function for DMRG ( $M = 920$ ), SHCI ( $\epsilon = 6 \times 10^{-6}$ ) and ICE-CI ( $T_{\text{Gen}} = 4 \times 10^{-5}$ ) (isovalue = 0.80). Relevant attractors are shown as **blue** spheres, and their electron populations and volumes are given, in units of electrons and cubed angstroms, respectively.

Figure S6 gives a comparison of CASSCF methods with different active spaces, comparing both ELF and difference density plots.



**Fig. S6** Plots of the electron localisation function for CASSCF with increasing active spaces (isovalue = 0.80) as well as difference density plots (w.r.t. RHF). Relevant attractors are shown as blue spheres, and their electron populations and volumes are given, in units of electrons and cubed angstroms, respectively.

### Natural orbital visualization

The natural orbitals associated with the various correlated wavefunctions are shown in Figures S7-S8. The near-Full-CI methods are shown in Figure S7 and reveal near-identical natural orbital shapes and occupation numbers.

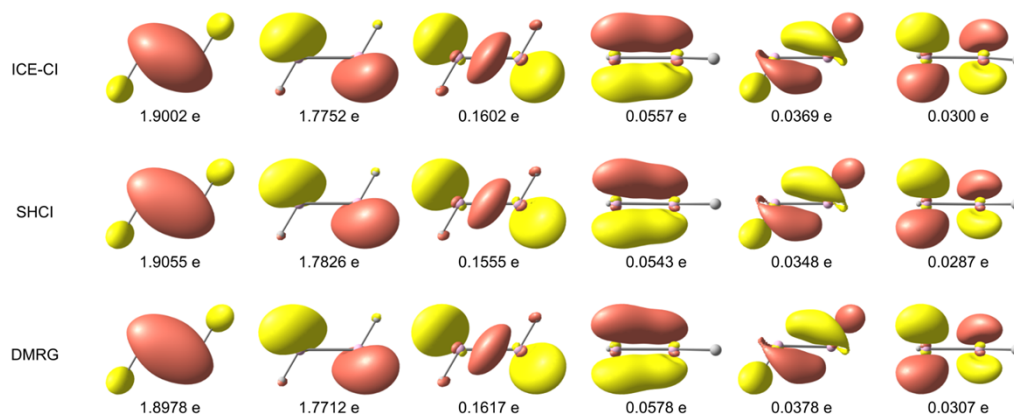


**Fig. S7** Visualisation of the selected natural orbitals of  $\text{Al}_2\text{H}_2$ , with occupations shown below each orbitals, for DMRG ( $M = 920$ ), SHCI ( $\epsilon = 6 \times 10^{-6}$ ) and ICE-CI ( $T_{\text{Gen}} = 4 \times 10^{-5}$ ). The orbitals were visualised using an isovalue of 0.05.

Figure S8 compares the valence natural orbitals of the simpler MP2, CC and CASSCF wavefunctions (comparing unrelaxed vs. relaxed densities in the case of MP2 and CCSD). MP2 is found to predict overall quite accurate NO shapes but predicts too low occupation numbers of the primary NOs, suggesting an underestimation of diradical character. CCSD meanwhile only mildly underestimates the NOs (but shows a slightly different shape of the orbital with occupation 0.1204). CCSD(T) gives close to quantitative accuracy of the NO

occupations and very similar NO shapes as the near-Full-CI NOs in Figure S7. CASSCF(4,5) gives qualitatively accurate results for the most important orbitals but shows the low occupation NO orbital being incorrect compared to Full-CI and the other methods.

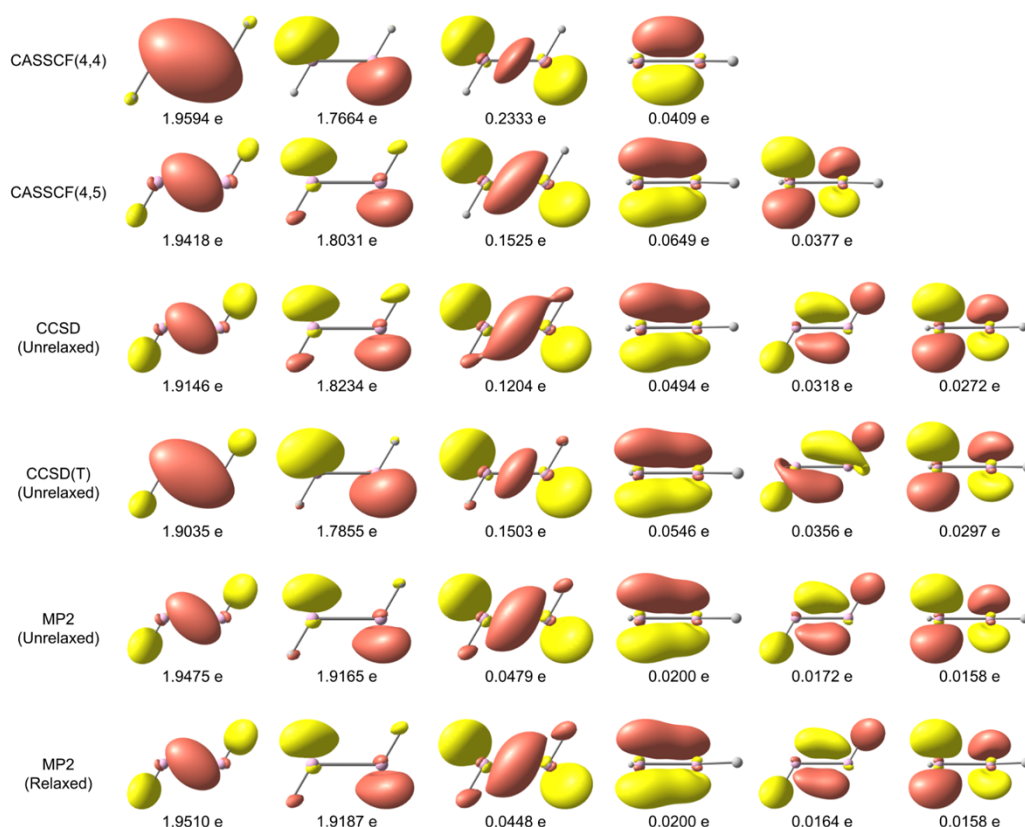


**Fig. S8** Visualisation of the primary natural orbitals of  $\text{Al}_2\text{H}_2$ , with occupations shown below each orbital, for selected methods. The orbital isosurfaces were visualised using an isovalue of 0.05.

## Mayer bond orders

Mayer bond orders were calculated for both correlated WFT methods and DFT methods as shown in Tables S3-S4.

**Table S3** Comparison of Mayer bond orders for selected correlated WFT methods that were tested.

Method	Mayer bond order
RHF	0.999
MP2	1.041
CCSD (Unrelaxed)	0.920
CCSD(T) (Unrelaxed)	0.900
CCSDT (Unrelaxed)	0.999
CASSCF(8,14)	0.852
MRCI+Q(8,14)	0.903

DMRG(8,86)	0.889
SHCI(8,86)	0.900
ICE-CI(8,86)	0.891

**Table S4** Comparison of Mayer bond orders for the density functionals that were tested.

Method	Mayer bond order
PBE	1.158
TPSS	1.133
r <sup>2</sup> SCAN	1.129
TPSSh	1.115
B3LYP	1.091
BHHLYP	1.042
M06-2X	0.993
$\omega$ B97X-V	0.998
B2PLYP	1.056
DSD-PBEP86	1.048

### Vertical singlet-triplet gaps of Al<sub>2</sub>H<sub>2</sub>

The vertical singlet-triplet gap (VSTG) of Al<sub>2</sub>H<sub>2</sub> was tested as an alternative energetic property to study WF convergence. We note, however, in agreement with Tuononen, that the lowest triplet Al<sub>2</sub>H<sub>2</sub> state is not related to the diradical character of the ground-state singlet as it is the pure  $\pi$ -bonding unoccupied orbital that becomes occupied in this case. See final section of ESI on the electronic states of Al<sub>2</sub>H<sub>2</sub> for more information.

Due to size-inconsistency errors in VSTGs likely being less severe than for bond dissociation energies, different trends were expected to emerge. The ICE-CI method was utilised to estimate the Full-CI/cc-pVTZ VSTG limit (Figure S9). Convergence was reached relatively quickly and smoothly as a function of the T<sub>Gen</sub> parameter, yielding a final Full-CI/cc-pVTZ estimate of 18.6 kcal mol<sup>-1</sup>.

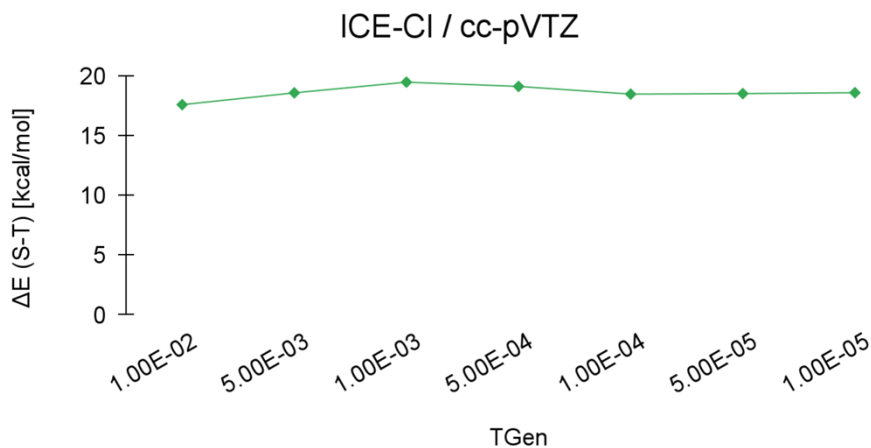


**Fig. S9** Estimation of vertical singlet-triplet gap of  $\text{Al}_2\text{H}_2$  using ICE-CI, as a function of the  $T_{\text{Gen}}$  threshold.

We can again compare simpler WFT and DFT methods against this Full-CI estimate, as shown in Figure S10. It is immediately clear that most WFT methods perform relatively well in predicting the VSTG, with some exceptions. Beginning with single-reference methods, HF performs very poorly, predicting a value of 3.3 kcal mol<sup>-1</sup>. MP2 performs moderately well, with a value of 17.6 kcal mol<sup>-1</sup>, demonstrating once again that the lack of a proper treatment of static correlation does not hinder the performance of this method as much as one might expect. Moving on to coupled cluster, excellent results are obtained, with the inclusion of only single and double excitations (CCSD) already underestimating the Full-CI estimate by only 0.1 kcal mol<sup>-1</sup>. No tangible improvement is observed upon going to CCSD(T), CCSDT or CCSDT(Q), with CCSDT and CCSDTQ giving an identical answer to one decimal place, while CCSD(T) actually overestimates by 0.3 kcal mol<sup>-1</sup>.

Moving on to the multi-reference methods, of which only the (4,5) active space was tested, an overestimation by CASSCF was observed, by 2.6 kcal mol<sup>-1</sup>. Interestingly, introducing dynamic correlation via MRCI+Q, the result actually worsened by a further 4.9 kcal mol<sup>-1</sup>. This was remedied by decreasing the value of the selection threshold parameter ( $T_{\text{Sel}}$ ) from the default  $1 \times 10^{-6}$  to  $1 \times 10^{-7}$  as well as zero, which then gave results that were on par with the coupled cluster results.

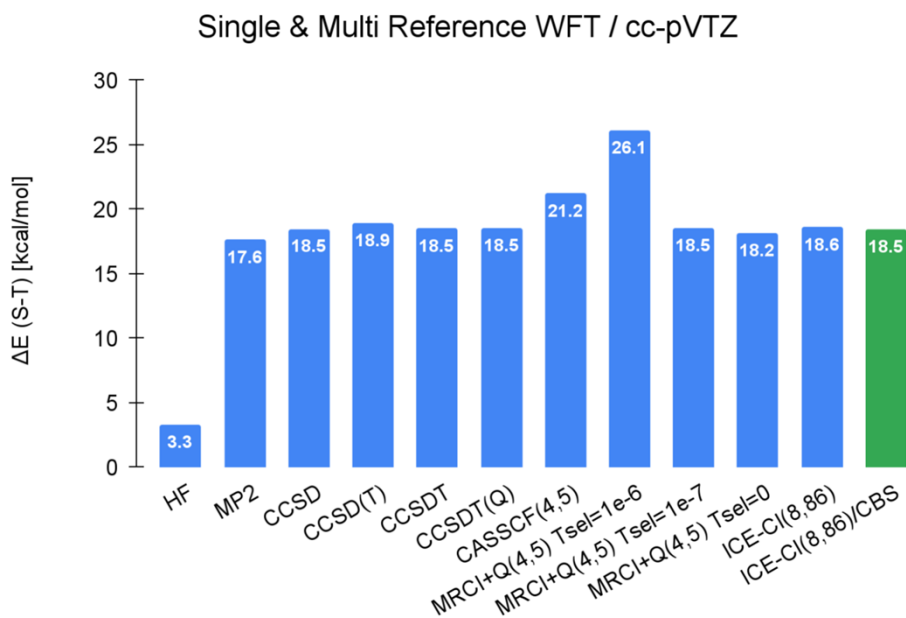


**Fig. S10** Performance of various single- and multi-reference correlated wavefunction theory methods in predicting the vertical singlet-triplet gap of  $\text{Al}_2\text{H}_2$  using the cc-pVTZ basis set. Additionally a -0.1 kcal/mol complete basis set (CBS) correction was derived using a basis set extrapolation of the vertical singlet-triplet gap using the cc-pVQZ and cc-pV5Z energies. A TZ→CBS correction of 1.62 kcal/mol (i.e. VSTG[4,5 Extrapolation] - VSTG[cc-pVTZ]) can be derived from these values.

A comparison of various density functionals were also tested in the prediction of the VSTG (Figure S11). A complete basis set (CBS) correction of -0.1 kcal mol<sup>-1</sup> was derived using CCSD(T)/CBS(4,5) extrapolations. Adding this correction to the ICE-CI/cc-pVTZ result gave an estimate of the VSTG at the ICE-CI/CBS limit (18.5 kcal mol<sup>-1</sup>). It was found that the (meta)-GGA functionals (PBE, TPSS and r<sup>2</sup>SCAN) underestimate the VSTG, with r<sup>2</sup>SCAN providing the worst result of 8.9 kcal mol<sup>-1</sup>. Introducing a small amount (10%) of HF exchange with TPSSh did not improve the situation. However, by going to higher amounts of HF exchange (B3LYP, M06-2X and  $\omega$ B97X-V), significant improvements were observed. In contrast to the results for the VBDE, no real gain is found by going to double-hybrid functionals, with B2PLYP performing similarly to  $\omega$ B97X-V, and DSD-PBEP86 performing worse. In summary, hybrid functionals appear to be required for a reliable spin-state energy gap, although one should also take into consideration the poor performance of some of these methods in predicting the electron density of singlet  $\text{Al}_2\text{H}_2$ .

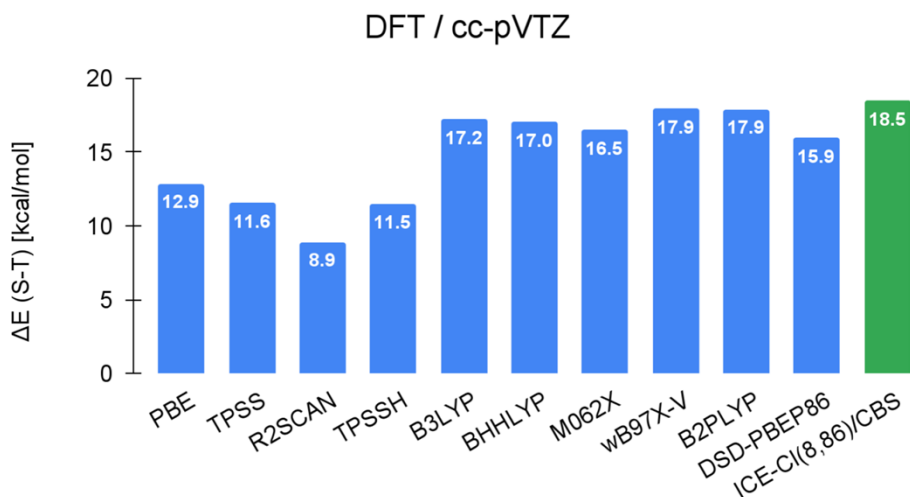


**Fig. S11** Performance of density functional theory in predicting the vertical singlet-triplet gap of  $\text{Al}_2\text{H}_2$ . The ICE-CI(8,86)/CBS result is included as a reference point, in green.

### Diradical character analysis

In the previous study carried out by Tuononen and coworkers<sup>1</sup>, the diradical character of the group 13 dimetallenes ( $\text{E}_2\text{R}_2$ ,  $\text{E} = \text{Al-Tl}$ ,  $\text{R} = \text{H, Me, }^i\text{Bu, Ph}$ ) was assessed by analysing the weights of the HF and doubly excited determinants from CASSCF(4,5) calculations. In a perfect singlet diradical, the HF and excited diradical determinants would have equal weights in the overall wavefunction, i.e. their CI coefficients would both be  $1/\sqrt{2}$ . The diradical character is then defined using the simple relation  $[2 \times C_{\text{DRCL}}^2 \times 100]$  (where  $C_{\text{DRCL}}$  is the CI coefficient of the doubly excited diradical determinant) to give the percentage diradical character. Tuononen found that the diradical character varied from approximately 14% for aluminium, dropping to  $\sim 1\%$  for thallium, as group 13 is descended. Interestingly, varying the substituent had little to no effect on the diradical character. The work carried out by Tuononen was, however, mostly limited to a CASSCF(4,5) WF. As discussed herein, such a multiconfigurational WF actually captures very little dynamic correlation. Here we utilize large active-space ICE-CI calculations to systematically explore how the diradical character using the CI-coefficient definition, varies as a function of active space size.

### Diradical character analysis via CI coefficients

In order to assess how the diradical character, as analysed via the CI coefficients of a CASSCF wavefunction, depends on active space, we systematically increased the active space in regular CASSCF calculations as well as ICE-approximated CASSCF calculations. The ICE-CI approximation allows us to go to much larger active spaces. The results are shown in Figure S12. Regular CASSCF calculations were feasible up until an active space of (8,14), whereas with the ICE-CASSCF method we could go to much larger active spaces.

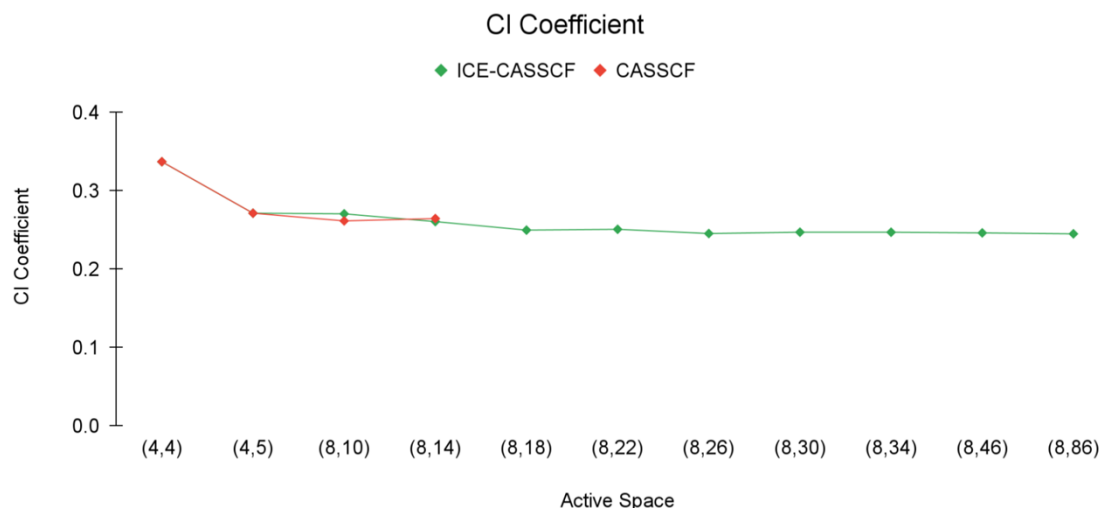


**Fig. S12** Variation of the diradical character of  $\text{Al}_2\text{H}_2$ , measured via the CI coefficient, as a function of increasing active space in CASSCF and ICE-CASSCF calculations. The ICE-CI Full-CI algorithm was used as a replacement for regular Full-CI algorithm in standard CASSCF, using a  $T_{\text{Gen}}$  value of  $10^{-4}$ .

In the regular CASSCF calculations, we see a decreasing trend upon going from a (4,4) active space to an (8,14) active space, with our calculations reproducing Tuononen's CASSCF(4,5) results. Increasing the (4,5) active space to (8,10) or (8,14) led to a small decrease in the CI coefficient by approximately 0.01, corresponding to about a 1% decrease in the diradical character predicted by Tuononen. The ICE-CI approximation ( $T_{\text{Gen}}$  threshold of  $1 \times 10^{-4}$ ) was found to reproduce the small active space CASSCF results well. As the active space was increased further, up to (8,86), the CI coefficient further decreased, predicting around 12% diradical character for ICE-CASSCF(8,86). This corresponds to around a 2%-value decrease in diradical character, in comparison to the results obtained when using a (4,5) active space.

Large active-space ICE-CASSCF calculations, however, quickly become unfeasible for larger molecules. An alternative CI-based WF method, to CASSCF, is to add a MRCI+Q dynamic correlation treatment on top. MRCI+Q also involves a diagonalization of a CI matrix, yielding CI coefficients and can also be used to define diradical character in a similar way. We tested this by performing MRCI+Q calculation on CASSCF(4,5) reference wavefunctions for the other group 13 transient dimetallenes,  $\text{E}_2\text{R}_2$  ( $\text{E} = \text{Al}, \text{Ga}, \text{In}, \text{Tl}$  and  $\text{R} = \text{H}, \text{Me}$ ) previously studied by Tuononen. Different selection thresholds ( $T_{\text{sel}}$ ) parameters were tested. Figure S13 compares CASSCF(4,5) and MRCI+Q CI coefficients.

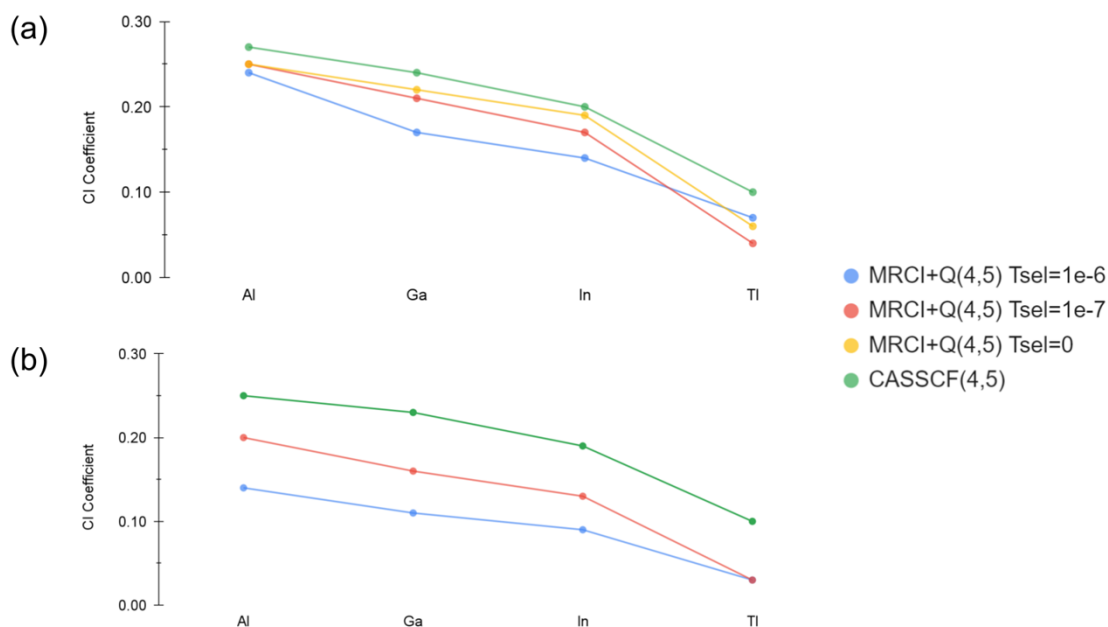


**Fig. S13** Comparison of the CASSCF(4,5) CI coefficient to the MRCI+Q(4,5) CI coefficient, calculated using decreasing values of the  $T_{\text{Sel}}$  selection parameter. (a) Hydride-substituted transient group 13 dimetallenes. (b) Methyl substituted transient group 13 dimetallenes.

Our CASSCF(4,5) calculations reproduce the CI coefficients and trends predicted by Tuononen reliably (Figure S13). The MRCI+Q results were found to be strongly dependent on the  $T_{\text{Sel}}$  parameter, with the default  $T_{\text{Sel}} = 1 \times 10^{-6}$  value giving unreliable results. A  $T_{\text{Sel}} = 1 \times 10^{-7}$  value proved more reliable, when compared against the datapoint calculated with  $T_{\text{Sel}} = 0$  (where affordable). Overall, the results suggest that the diradical character initially predicted by CASSCF(4,5) using CI coefficients, is only mildly overestimated owing to the small size of the active space when compared to the large-active ICE-CI CASSCF calculations herein.

#### Diradical character analyzed via natural orbital occupations

More generally, however, any CI-coefficient based definition of diradical character is not ideal due to the dependence on a specific orbital set used in the CI or CASSCF calculation. In the case of CASSCF, different orbital representations are possible (though natural orbitals are a natural choice) and additionally the orbitals are redefined with each active space selection. Post-HF approaches utilize another orbital set, usually the HF orbitals. A more general diradical definition can be derived using natural orbitals (NO), which would offer the advantage of being a transferable definition across all WFT methods (as long as natural orbitals can be defined via diagonalization of a correlated 1-particle density matrix). A simple NO-based metric was previously discussed by Tuononen using the QCISD(T) and CASSCF(4,5) methods. The NO population of the major populated virtual orbital, was found to follow the same trend as observed for the CI vector coefficient metric for different species.

The advantage of NO-based metrics is that one can analyze the changes to the NOs as the wavefunction complexity changes, giving insight into both diradical character and overall WF quality. Figure S14 (and S15) compares the natural orbital occupation numbers (NOONs) obtained from different single and multireference WFs. It is found that CCSD(T) and MRCI+Q natural occupations are very close to ICE-CI occupations (here used as a Full-CI reference) with slightly larger deviations seen for CCSD. Meanwhile occupations from MP2 (unrelaxed or relaxed densities) show larger deviations, predicting less diradical character. Overall, the results suggest that the coupled cluster methods are capable of giving an accurate description of the diradical character in  $\text{Al}_2\text{H}_2$ , while MP2 does not fully capture these effects. Isosurfaces of the NO's are shown in Figures S7 and S8; they reveal that while the NO shapes predicted by MP2 are qualitatively correct (similar to CCSD), the populations of the primary NOs are too low in magnitude, as previously discussed by Tuononen.

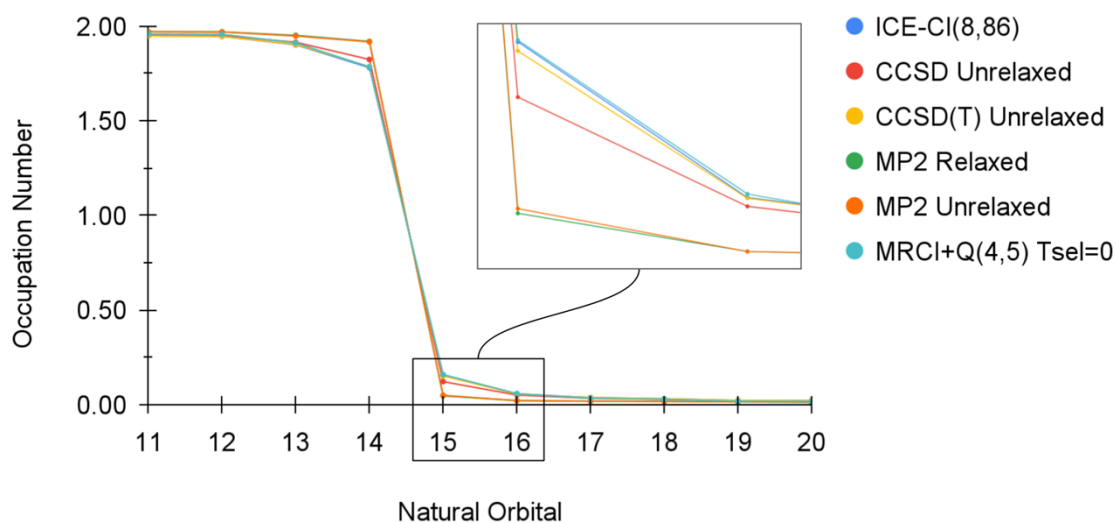


**Fig. S14** Plots of NO occupation numbers of  $\text{Al}_2\text{H}_2$  for selected methods (using the cc-pVTZ basis set). The plots begin at orbital number 11 (first correlated orbital), and end at orbital number 20 (where the occupation number becomes negligible). Figures S7-S8 shows isosurfaces of the NO's while Figure S15 shows a plot of all occupation numbers for the same methods.

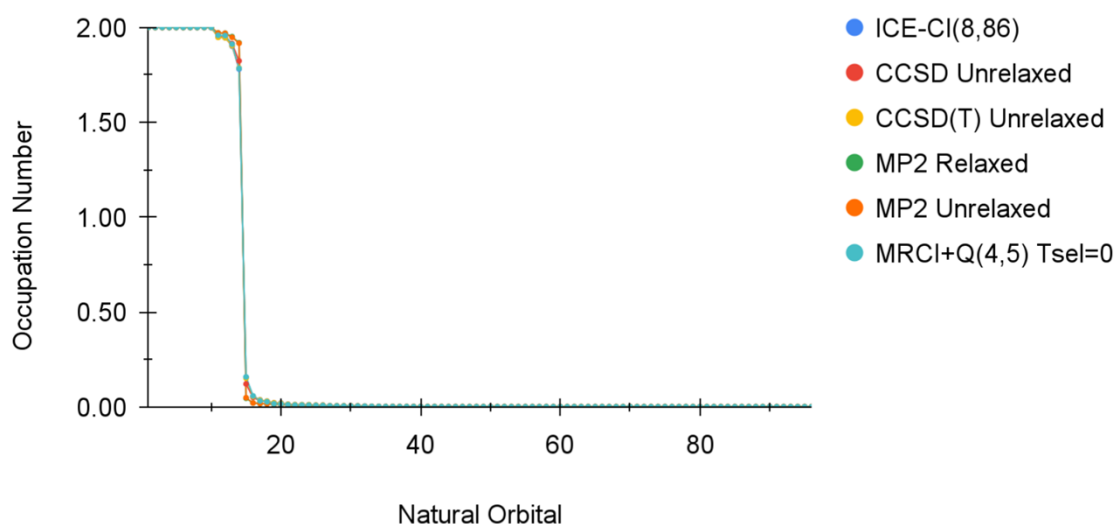


**Fig. S15** Plot of all natural orbital occupation numbers of  $\text{Al}_2\text{H}_2$  for selected methods (cc-pVTZ basis set). All 96 orbitals are shown, of which 10 occupied orbitals are frozen.

The single-NO based metric is useful for a simple molecule possessing diradical character. A more general NO-based metric (labelled HG-2), that does not require *a priori* understanding of the system, was defined by Head-Gordon.<sup>56</sup> The metric defines the number of effectively unpaired electrons in a molecule from the same natural orbitals and is effectively a measure of polyradical character in any molecule. The metric is simply calculated from the array of natural orbital occupation numbers using the simple functional form:

$$n_{u,nl} = \sum_i n_i^2 (2 - n_i)^2$$

where  $n_i$  is the occupation number of each particular natural orbital. Almost fully occupied natural orbitals ( $\sim 2.0$ ) or almost empty orbitals ( $\sim 0.0$ ) effectively make no contribution to  $n_{u,nl}$ . While this is not a unique metric (many definitions are possible), this equation has empirically found to be reliable (i.e. without producing values inconsistent with chemical intuition<sup>57</sup>).

Figure S16 compares various metrics for diradical character for the group 13 dimetallenes,  $\text{E}_2\text{R}_2$ ,  $\text{E} = \text{Al-Tl}$ ,  $\text{R} = \text{H, Me}$ . The plots suggest that a precise useful metric of diradical character may be difficult, due to the sensitivity w.r.t metric employed as well as the theory-level used. Overall, in agreement with Tuononen et al., diradical character decreases as group 13 is descended.

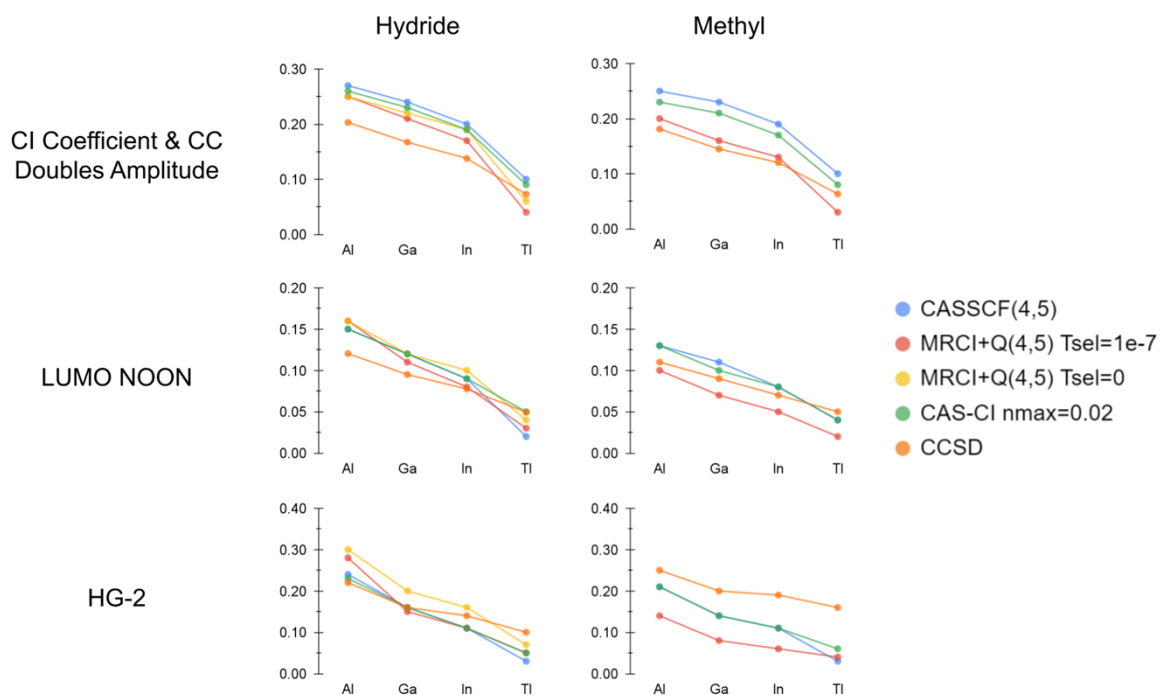


**Fig. S16** Diradical character of the hydride- and methyl-substituted group 13 dimetallenes, measured via the CI coefficient, coupled cluster doubles amplitude, LUMO natural orbital occupation number and the polyradical Head-Gordon index (HG-2).

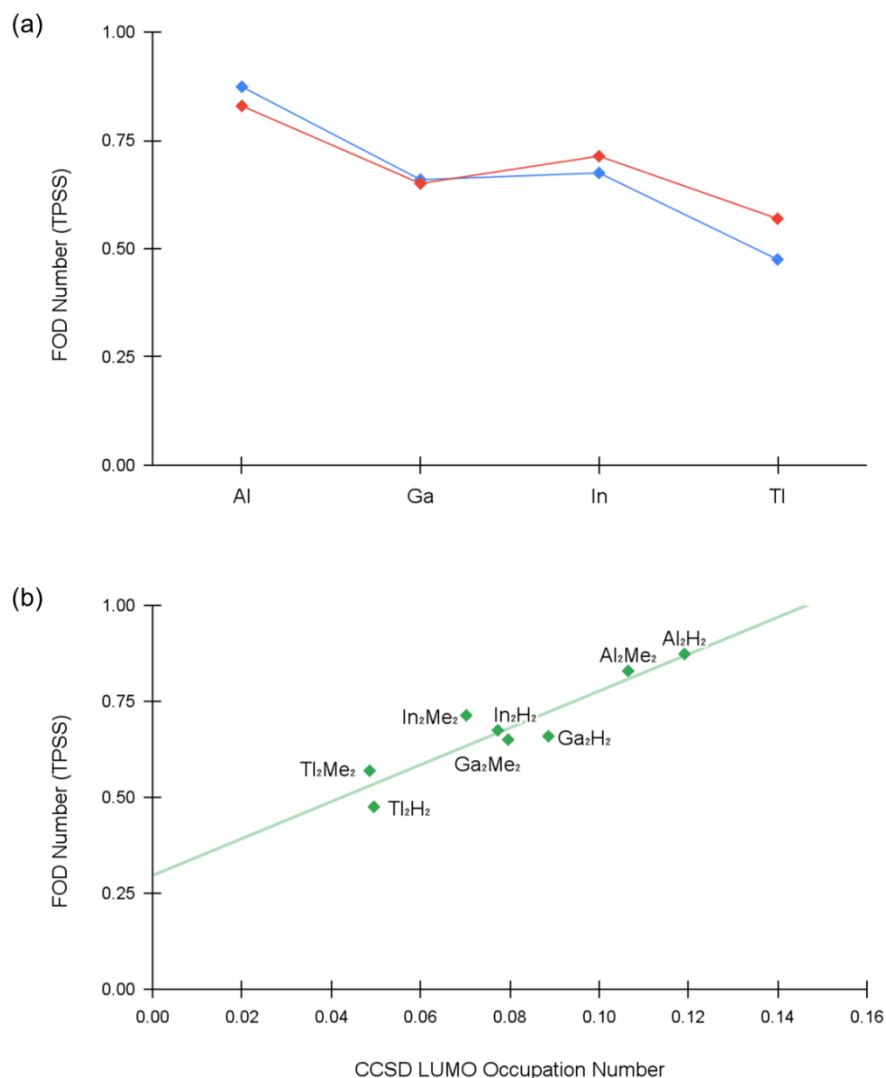


**Fig. S17** Alternative version of Fig 11 in manuscript using an all-electron Douglas-Kroll-Hess Hamiltonian and cc-pVTZ-DK basis set for all elements. Note that the values for the Ga species shift the most compared to Fig. 11. (a) Diradical character of the hydride- and methyl-substituted group 13 dimetallenes, measured via the calculation of the number of “hot” electrons, the FOD number ( $N^{\text{FOD}}$ ). The FOD analysis was carried out at the FT-TPSS/cc-pVTZ-DK ( $T_{\text{el}} = 5000$  K) level of theory. (b) Scatter plot showing correlation of the TPSS-calculated FOD number with the natural occupation of the LUMO calculated at the CCSD/cc-pVTZ-DK (unrelaxed density) level, for the same transient group 13 dimetallenes studied.

### Density-driven vs. functional-driven analysis

Table S5 shows the vertical bond dissociation energy of different functionals and the error with respect to the FCI/CBS estimate, decomposed into the functional-driven (FE) and density-driven error (DE).

**Table S5** Reaction energies and errors w.r.t the WFT reference. The reaction energy errors are decomposed into functional-driven (FE) and density-driven errors in kcal/mol. The FCI/CBS reference reaction energy is defined as the DMRG/cc-pVTZ-calculation + CCSD(T)/CBS(4,5) correction. The reference density was calculated at the CCSD(T)/cc-pVTZ level of theory (as a good approximation to the exact density) to evaluate the FE and DE terms (see equations in manuscript).

	$\Delta E$	Error (kcal/mol)	FE (kcal/mol)	DE (kcal/mol)
Reference (FCI/CBS)	18.4	-	-	-
B3LYP	15.67	-2.73	-2.53	-0.20
BHLYP	13.04	-5.36	-6.45	1.09
CAM-B3LYP	13.40	-5.00	-5.43	0.42
HF	5.83	-12.57	-17.30	4.73
LDA	28.39	9.99	10.55	-0.56
M06-2X	14.77	-3.63	-5.05	1.42
PBE	23.44	5.04	5.48	-0.44
PBE0	20.99	2.59	2.37	0.22
r <sup>2</sup> SCAN	24.76	6.36	6.39	-0.03
TPSS	21.92	3.52	3.55	-0.03
TPSSh	21.05	2.65	2.47	0.18
$\omega$ B97X-V	15.15	-3.25	-4.76	1.51

Table S6 compares for the same DFT methods as in Table S6, the integrated volume of positive difference density plots, ELF Al-Al basin population as well as the ELF error of the same basis (relative to the DMRG ELF Al-Al basin).

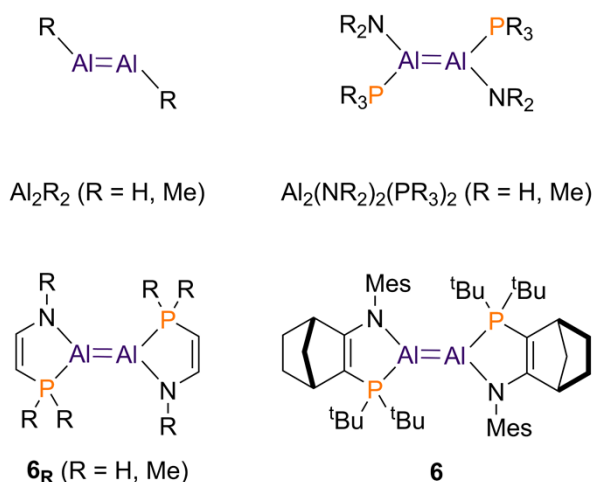
**Table S6** Integrated volume of the positive difference densities and ELF population (Al-Al basin) errors, referenced against the FCI reference (DMRG).

	Int. Vol. Pos. Diff. Dens.	ELF Al-Al Pop. [e]	ELF Error
Ref. (DMRG)	-	1.16	-
B3LYP	0.14	0.88	-0.28
BHLYP	0.13	0.68	-0.48
CAM-B3LYP	0.16	0.64	-0.52

HF	0.18	0.25	-0.91
LDA	0.23	0.98	-0.18
M06-2X	0.15	0.42	-0.74
PBE	0.15	0.99	-0.17
PBE0	0.11	0.83	-0.33
r <sup>2</sup> SCAN	0.09	0.99	-0.17
TPSS	0.11	0.97	-0.19
TPSSh	0.10	0.91	-0.25
ωB97X-V	0.15	0.42	-0.74

## Structures of Al<sub>2</sub>H<sub>2</sub> and other dialumenes

Geometries of Al<sub>2</sub>H<sub>2</sub> and other dialumenes (Scheme S1) were calculated using various DFT methods, with and without dispersion corrections. The Al-Al bond distances are shown in Table S7. The Al-Al distance in the dialumenes is found to depend primarily on the ligand, becoming shorter with increased ligand size. Overall, for Al<sub>2</sub>H<sub>2</sub>, all methods are capable of satisfactory accuracy (compared to a reference value of 2.644 Å, estimated from ICE-CI, see Table S9). This reveals that the behaviour of different methods for capturing diradical character or electron density does not translate into appreciably different structural parameters. For the larger dialumenes, however, a larger difference between methods can be seen (compare e.g. TPSS vs. TPSS-D), revealing that treatment of dispersion becomes more important for accurately capturing the local structure of large dialumenes. We note that M06-2X is known to be capable of treating some dispersion directly via its functional form, which explains its satisfactory performance for larger dialumenes, even when carried out without a dispersion correction.



**Scheme S1** Set of dialumenes (transient and base-stabilised) that were studied (Mes = 2,4,6-trimethylphenyl).

**Table S7** Comparison of the Al-Al bond distance [Å] of the dialumenes in Scheme S1, optimised using three functionals of increasing HF exchange, with and without dispersion.

Structure	TPSS	TPSS-D3	TPSS-D4	TPSS-NL	B3LYP	B3LYP-D3	M06-2X	M06-2X-D3
$\text{Al}_2\text{H}_2$	2.646	2.644	2.642	2.636	2.677	2.673	2.669	2.670
$\text{Al}_2\text{Me}_2$	2.698	2.691	2.689	2.687	2.748	2.735	2.758	2.758
$\text{Al}_2(\text{NH}_2)_2(\text{PH}_3)_2$	2.631	2.636	2.627	2.618	a <sub>-</sub>	a <sub>-</sub>	a <sub>-</sub>	a <sub>-</sub>
$\text{Al}_2(\text{NMe}_2)_2(\text{PMe}_3)_2$	2.591	2.585	2.580	2.590	2.618	2.603	2.632	2.633
$\mathbf{6}_H$	2.580	2.572	2.566	2.566	2.642	2.625	2.655	2.655
$\mathbf{6}_{Me}$	2.551	2.540	2.536	2.539	2.580	2.561	2.581	2.579
$\mathbf{6}$	2.563	2.516	2.511	2.519	2.595	2.527	2.536	2.535

<sup>a</sup> Complete dissociation of the base from the dialumene,  $\text{PH}_3$ , occurred when attempting to optimize the geometries using the two hybrid functionals.

Table S8 compares MP2 calculations (DLPNO-MP2 for the full complex **6**) for dialumenes of increasing size as well as CCSD and CCSD(T) calculations for the smaller  $\text{Al}_2\text{H}_2$  and  $\text{Al}_2\text{Me}_2$  species. There is overall good agreement between MP2 and CCSD(T) for  $\text{Al}_2\text{H}_2$  (despite the diradical character not being well described at the MP2 level) that one would expect MP2 to be a reasonably accurate structural optimization method for the larger complexes. For the full complex **6** there is also good agreement between MP2 and the dispersion-corrected DFT methods in Table S7. For  $\text{Al}_2\text{H}_2$ , we additionally carried out higher-order CC calculations at the CCSDT level of theory, which reduced the Al-Al bond length to 2.647 Å.

**Table S8** Comparison of the Al-Al bond distance [Å] of the studied dialumenes, optimised using MP2, CCSD and CCSD(T), where feasible. The geometry optimizations were carried out using the cc-pVTZ basis set.

Structure	MP2	CCSD	CCSD(T)	CCSDT
$\text{Al}_2\text{H}_2$	2.651	2.657	2.654	2.647
$\text{Al}_2\text{Me}_2$	2.715	2.723	2.700	

$\text{Al}_2(\text{NH}_2)_2(\text{PH}_3)_2$	2.627	-	-
$\text{Al}_2(\text{NMe}_2)_2(\text{PMe}_3)_2$	2.565	-	-
<b>6<sub>H</sub></b>	2.590	-	-
<b>6<sub>Me</sub></b>	2.537	-	-
<b>6</b>	<sup>a</sup> 2.515	-	-

<sup>a</sup>The DLPNO-MP2 approximation was employed, and the C and H atoms were treated with the cc-pVDZ basis set to reduce computational cost.

In order to estimate the Al-Al bond length in the Full-CI limit (with the cc-pVTZ basis set), we carried out ICE-CI-CASSCF geometry optimizations. This was done by performing CASSCF calculations using a complete orbital space (within the frozen-core approximation) of CAS(8,86) but using the ICE-CI selected-CI solver instead of exact Full-CI solver and varying the  $T_{\text{Gen}}$  selection threshold systematically. The ICE-CI CASSCF calculations were found to converge convincingly with decreasing  $T_{\text{Gen}}$  threshold, to give an optimized Al-Al bond length of 2.644 Å at  $T_{\text{Gen}} = 7 \times 10^{-4}$  that remained unchanged at  $T_{\text{Gen}} = 2 \times 10^{-4}$ . We estimate the 2.644 Å bond length to be of Full-CI/cc-pVTZ quality.

**Table S9** Comparison of the Al-Al bond length [Å] of  $\text{Al}_2\text{H}_2$  calculated with ICE-CI-CASSCF with a full orbital space (within frozen-core approximation) of CAS(8,86) and with varying TGen thresholds

$T_{\text{gen}}$	Al-Al bond length (Å)
5E-1	2.643
1E-1	2.642
5E-2	2.642
1E-2	2.644
5E-3	2.643
1E-3	2.643
7E-4	2.644
5E-4	2.644
4E-4	2.644
3E-4	2.644
2E-4	2.644

It is also of interest to compare how the Al-Al bond length converges for CASSCF wavefunctions with varying active spaces. This is shown in Table S10 and it shows that CASSCF calculations (utilizing the ICE-CI approximation with  $T_{\text{Gen}}=1 \times 10^{-4}$  for the larger active spaces) show somewhat slow convergence towards the Full-CI limit but start to give

acceptable accuracy once a CAS(8,30) active space is reached. This suggests that dynamic correlation effects are important for obtaining an accurate Al-Al bond length.

**Table S10** Comparison of the Al-Al bond distance [ $\text{\AA}$ ] of  $\text{Al}_2\text{H}_2$  calculated with CASSCF wavefunctions with varying active-spaces. Basis set: cc-pVTZ. ICE-CASSCF calculations used  $T_{\text{Gen}}=1 \times 10^{-4}$ .

Method	Al-Al distance ( $\text{\AA}$ )
RHF	2.783
CASSCF(4,4)	2.622
CASSCF(4,5)	2.681
CASSCF(8,10)	2.740
CASSCF(8,14)	2.707
CASSCF(8,18)	2.663
ICE-CASSCF(8,18)	2.662
ICE-CASSCF(8,22)	2.662
ICE-CASSCF(8,26)	2.665
ICE-CASSCF(8,30)	2.652
ICE-CASSCF(8,34)	2.649
ICE-CASSCF(8,46)	2.648

## Electronic states of $\text{Al}_2\text{H}_2$

To shed light on the electronic states available to the  $\text{Al}_2\text{H}_2$  molecule, additional multireference calculations were carried out using ORCA version 6.0. In order to calculate the lowest electronic states without bias, we turned to state-averaged multireference calculations. An active space of CAS(4,5) was used and the CASSCF problem was solved for three  $S=0$  and two  $S=1$  states simultaneously. The natural orbitals and occupations for this active space is shown in Fig S18.

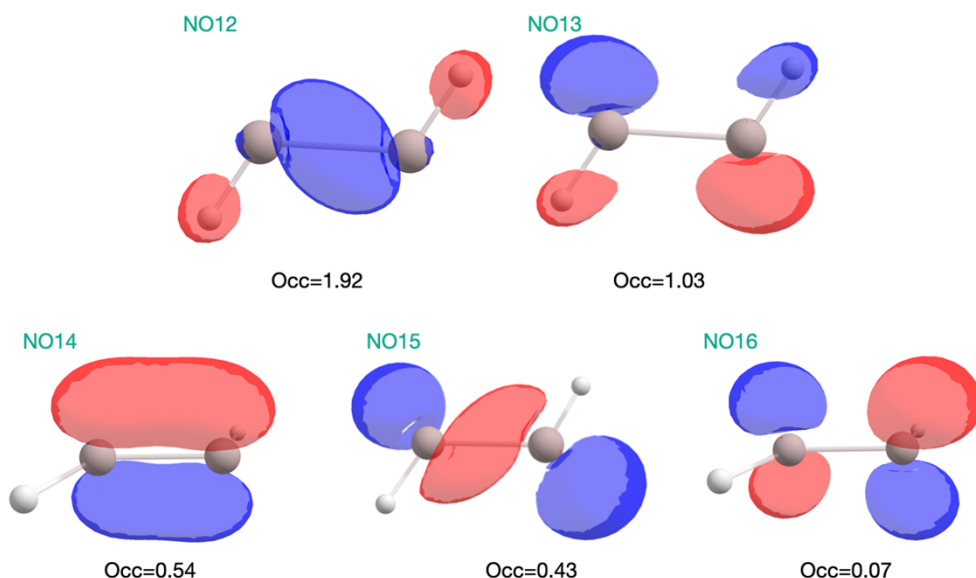


**Fig. S18** The active space orbitals of state-averaged CASSCF(4,5) WF including 3 singlet roots and 2 triplet roots. The occupations are state-averaged. Note that the active-space order (ordered by NO occupations) is different from Fig. S7 and S8.

Table S11 shows the relative energies as well as the weights and configurations of the 3 lowest singlet states and the 2 lowest triplet states at the CASSCF(4,5) level with and without dynamic correlation contributions from NEVPT2 and FIC-MRCC.

**Table S11.** The lowest energy singlet and triplet states from the SA-CASSCF(4,5) calculations shown as dominant configurations (and respective weights). The configurations refer to the orbitals in Fig. S18 with same order. Also shown are relative energies at CASSCF, NEVPT2 and FIC-MRCC levels of theory.

State and major CFGs	CASSCF	NEVPT2	FIC-MRCC
S=0, root 0	0.0	0.0	0.0
0.851 22000 0.106 20020			
S=0, root 1	36.3	31.4	30.7
0.882 21100 0.056 20011			
S=0, root 2	63.0	61.3	58.1
0.592 20110 0.261 21001			
S=1, root 0	17.8	18.7	19.0
0.911 21100 0.043 11110			
S=1, root 1	25.1	27.5	26.8
0.964 21010 0.015 11020			

As expected, the lowest energy singlet state ( $S=0$ , root 0) is the diradicaloid state discussed in the manuscript. This state is dominated by the closed-shell configuration (22000, weight of 0.851), which corresponds to the 4 electrons occupying NO12 and NO13 in Fig. S18. The diradical character in the state comes from the 0.106 contribution of the 20020 configuration. This corresponds to a double excitation from NO13 to NO15.

The next singlet state lies considerably higher in energy (36.3, 31.4 and 30.7 kcal/mol at the SA-CASSCF, NEVPT2 and FIC-MRCC levels). This state is dominated by the 21100 configuration which corresponds to a single excitation from NO13 to NO14. We interpret this state as a diradical state but since it involves a different unoccupied orbital (NO14) than the double excitation in the ground-state singlet (NO13), this state is not related to the diradical character in the ground state.

The third singlet state lies 63 kcal/mol higher in energy at the CASSCF level. While this state does occupy NO13 to some extent, it is found to be highly multiconfigurational and is hard to interpret.

The lowest-energy triplet state is the lowest-energy excited state of this system. It is 17.8 kcal/mol higher in energy than the ground-state singlet at the CASSCF level (18.7 and 19.0 kcal/mol at NEVPT2 and FIC-MRCC). These energies are in good agreement with Full-CI/CBS estimate of 18.6 kcal/mol of the singlet-triplet gap of  $\text{Al}_2\text{H}_2$  previously mentioned. Interestingly, this state is found to primarily arise from a single (spin-flipped) excitation from NO13 to NO14. It is thus related to the first excited singlet state ( $S=0$ , root 1) and not the ground-state singlet (as the diradical configuration in the ground state involves NO15).

A higher excited triplet state lies at 25.1/27.5/26.8 kcal/mol (CASSCF/NEVPT2/FIC-MRCC) above the ground-state singlet. This triplet state is found to be dominated by a single excitation from NO13 to NO15 and hence corresponds to a diradical triplet state that is directly related to the diradical character in the ground-state singlet that also involves NO15.

The state-averaged CASSCF calculations were also solved for more roots but other relevant electronic states were not encountered. State-specific calculations were also tested where weights in the multi-root CASSCF procedure were adjusted to allow the MOs to optimize for each specific state. Similar results could be obtained as in the SA-CASSCF calculations but the SA-CASSCF results were overall easier to interpret (as a common set of MOs can be discussed).

The excited state calculations of  $\text{Al}_2\text{H}_2$  reveal that the diradical character in the ground state cannot so easily be related to the available excited states of the molecule. The excited states are first of all quite high in energy (not easily populated in an experiment) and the lowest energy states are unrelated to the diradical character in the ground-state. For example, an experimental observation of the singlet-triplet gap would not be sufficient to correlate with the diradical character of the ground-state as one would have to distinguish the 2 lowest energy triplet states as only the higher energy one involves a relevant orbital configuration. Furthermore, an open-shell singlet with a relevant orbital configuration to the diradical configuration in the ground-state could not be found.

## Effect of solvent polarization on FOD plots

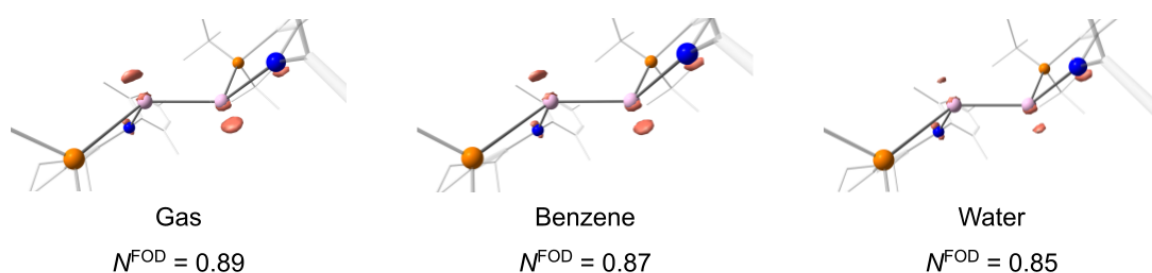


**Fig. S19** Visualisation of the fractional occupation weighted density of **6** at an isovalue of 0.005 a.u. and a grid of 120, in the absence and presence of a polarizable continuum model (CPCM). The FOD numbers ( $N^{\text{FOD}}$ ) are shown below each visualisation. The FOD analysis was carried out at the FT-TPSS/cc-pVTZ ( $T_{\text{el}} = 5000$  K) level of theory.